FATIGUE STRENGTH PREDICTION OF DUCTILE IRONS SUBJECTED TO COMBINED LOADING

M. Endo

Department of Mechanical Engineering, FukuokaUniversity,
Jonan-ku, Fukuoka 814-0180, Japan

ABSTRACT

The fatigue strength of ductile iron is influenced by small defects such as graphite nodules and microshrinkage cavities existing in the structure. Rotating bending and combined axial and torsional fatigue tests were carried out on round-bar smooth JIS FCD400, FCD600 and FCD700 specimens. A criterion for multiaxial fatigue failure of specimen with small defects is presented based on the observational results that the fatigue limit of specimens subjected to in-phase multiaxial stress is determined by the threshold condition for propagation of a mode I crack emanating from small defects. Using this criterion and the $\sqrt{area}$ parameter model, a method is proposed that enables one to predict the lower bound of fatigue limit of ductile irons by quantifying the effects of small defects and matrix structures without a fatigue test. The experimental results are in good agreement with the results predicted by the method.

INTRODUCTION

Ductile iron is cast iron in which small natural defects are present in the structure. Because of graphite nodules, the fatigue strength is lower than that of defect-free steel with the same matrix hardness [1]. Also, other small matrix discontinuities such as shrinkage cavities frequently cause both reduction and scatter in fatigue strength [2,3].

Murakami and Endo [4] proposed a geometrical parameter $\sqrt{area}$ for two-dimensional and three-dimensional defects on the basis of both microscopic observation of cracking from small defects at fatigue thresholds and three-dimensional numerical analysis of cracks with various shapes. $\sqrt{area}$ is defined as the square root of the area obtained by projecting a defect or crack onto the plane perpendicular to the maximum tensile stress. As a parameter representative of effect of matrix, they chose the Vickers hardness *HV* and finally proposed the following equation predicting the uniaxial fatigue limit σ_w of metals containing small defects without a fatigue test [5].

$$\sigma_w = 1.43\,(HV + 120) \,/\, (\sqrt{area}\,)^{1/6} \tag{1}$$

where σ_w is in MPa, *HV* is in kgf/mm^2 and $\sqrt{area}$ is in μm. In spite of the simplicity, this equation predicts the fatigue limit within the error of ~10 percent for defects and cracks having $\sqrt{area}$ less than 1000 μm and for *HV* ranging from 70 to 720. This model is called the $\sqrt{area}$ parameter model.

The $\sqrt{area}$ parameter model has successfully been applied to many problems related to uniaxial fatigue strength.

The extended application of this model to multiaxial fatigue problems has been discussed recently [6,7]. The author proposed a criterion for fatigue failure of metal specimens with a surface defect subjected to combined loading [7]. In this paper, the applicability of the $\sqrt{area}$ parameter model and this criterion to ductile irons will be discussed. The objective of the present study is to propose a method that enables one to predict the fatigue strength under combined loading without a fatigue test.

MATERIALS AND EXPERIMENTAL PROCEDURE

Three kinds of as-cast ductile irons: JIS FCD400, FCD600 and FCD700 were used. The chemical composition and mechanical properties are given in Table 1. The microstructures are shown in Figure 1. FCD400 is ferritic ductile iron with 14 % graphite nodules in a white ferrite matrix. FCD600 is cast iron with a typical bull's-eye structure of 14 % graphite nodules in envelopes of 46 % ferrite in a 40 % dark pearlite matrix. FCD700 is pearlitic ductile iron with 13 % graphite nodules in a matrix of 62 % pearlite and 25 % ferrite.

TABLE 1
CHEMICAL COMPOSITION AND MECHANICAL PROPERTIES

	C	Si	Mn	P	S	Mg	Cu	UTS, MPa	Elongation, %	Vickers hardness (10 kg)
FCD400	3.72	2.14	0.32	0.008	0.018	0.038	0.04	418	25.0	141
FCD600	3.76	2.98	0.14	0.23	0.015	0.052	0.30	641	14.1	216
FCD700	3.77	2.99	0.44	0.023	0.11	0.058	0.47	734	8.0	241

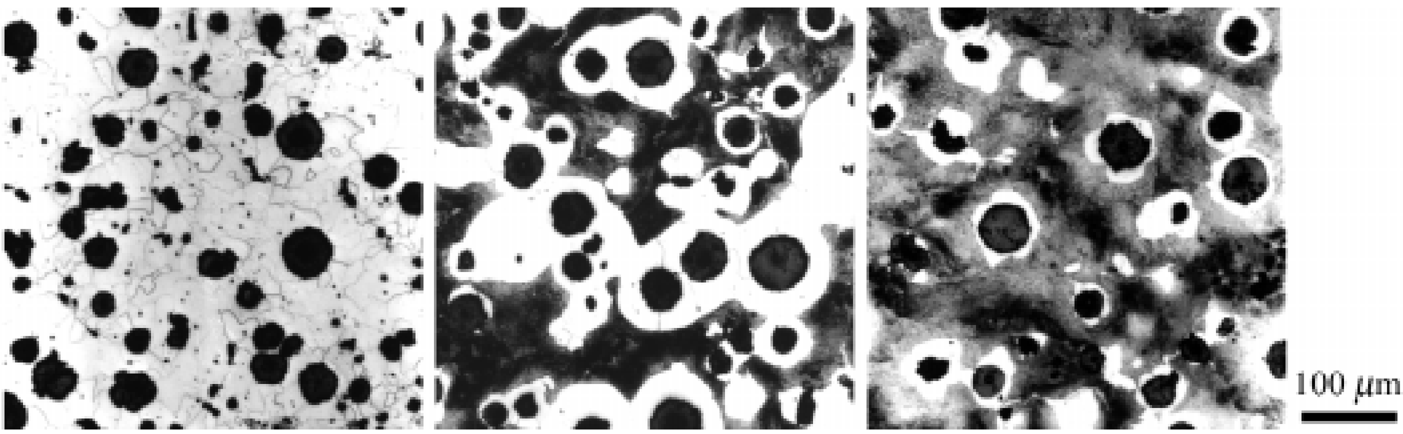

FCD400 FCD600 FCD700

Figure 1: Microstructures

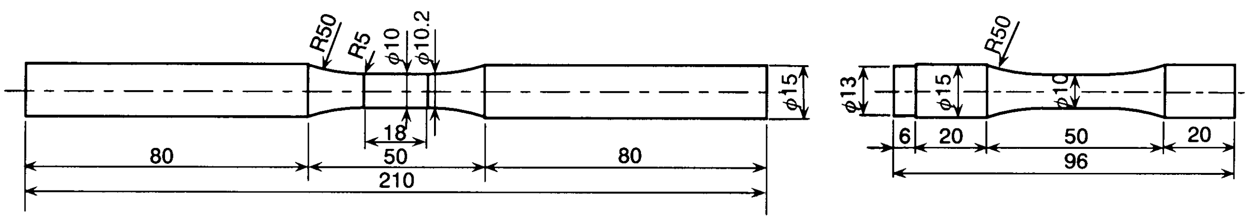

Figure 2: Dimensions of specimens for rotating bending (*left*) and axial/torsional load (*right*) tests

Specimens shown in Figure 2 were made by turning and milling. After surface finishing with an emery paper of grade #1000, about 30 μm of surface layer was removed by electropolishing. Surface graphite nodules and other defects will grow into greater pits than the original size during electropolishing. To remove these pits, the specimen surface was finished with alumina paste to the depth of about 10 μm and thereafter a thickness of 1 to 2 μm was removed from the surface layer by the second electropolishing.

Uniaxial load tests were carried out on a rotating bending testing machine of uniform moment type, with operating speed of 57 Hz. For combined axial and torsional load tests and pure torsion tests, an MTS digitally controlled servo-hydraulic fatigue testing machine was used at 30 to 45 Hz. The combined loading ratios of shear to normal stress amplitude were $\tau/\sigma = 0$ (rotating bending), 1 (combined loading) and infinity (pure torsion). All tests were performed under the condition of in-phase fully reversed ($R = -1$) constant amplitude loading with a sinusoidal waveform.

The fatigue limits σ_e and τ_e under combined stress are defined as the combination of the maximum nominal stresses under which a specimen endured 10^7 cycles for a fixed ratio τ/σ.

SMALL CRACK BEHAVIOUR AT FATIGUE LIMIT

It has previously been reported that the fatigue limit of nodular irons is related to a small crack propagation phenomenon [2,8]. Figure 3 shows the non-propagating cracks emanating from graphite nodules, which were observed on the specimen surface subjected to combined loading at the fatigue limit. It is worth noting that the direction of non-propagating cracks is approximately normal to the principal stress σ_1. This phenomenon was observed also in rotating bending and pure torsion tests. Under a stress slightly higher than the fatigue limit, a crack propagating in the direction normal to σ_1 led the specimen to break. In a previous work [7], fatigue tests were carried out for various combined loading ratios using annealed low carbon steel specimens containing a small artificial hole, and it was reported that the fatigue limit was determined by a crack emanating from the hole in the direction normal to σ_1, regardless of combined loading ratio.

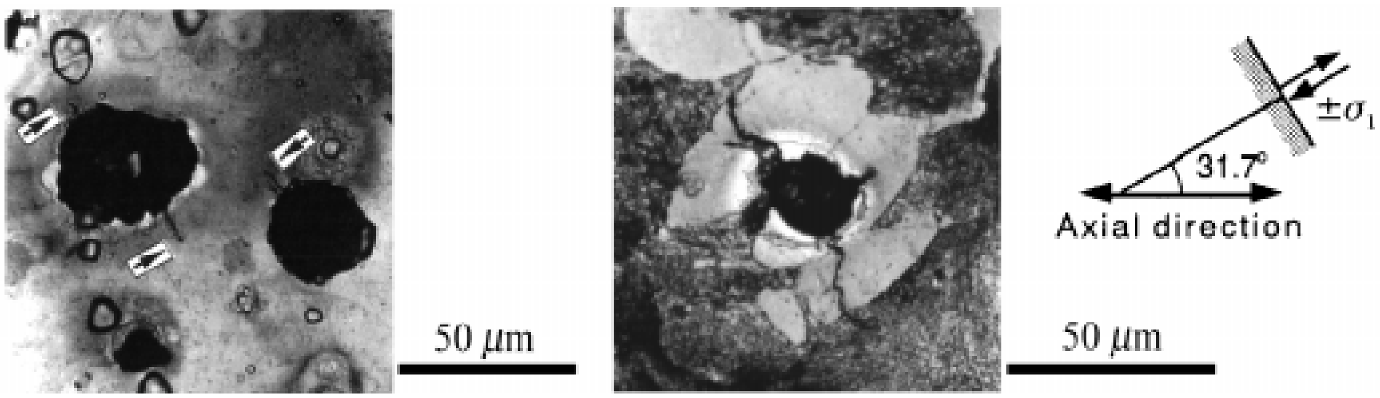

(a) FCD400; $\tau_e/\sigma_e = 1$
($\tau_e = \sigma_e = 120$ MPa)

(b) FCD700; $\tau_e/\sigma_e = 1$
($\tau_e = \sigma_e = 160$ MPa)

Figure 3: Non-propagating cracks observed at fatigue limit

CRITERION AND PREDICTIVE EQUATION

The above observational result makes one think of a model that fatigue limit problem of defect specimen under combined loading is equivalent to a fatigue threshold problem of a mode I crack emanating from a defect subjected to the maximum principal stress σ_1 normal to the crack and simultaneously to the minimum principal stress σ_2 parallel to the crack. Based on this model, a criterion for fatigue failure of specimens with a small defect was proposed as [7],

$$\sigma_1 + k\sigma_2 = \sigma_w \tag{2}$$

where σ_1 and σ_2 are the maximum and minimum principal stress amplitudes, σ_w is the uniaxial fatigue limit stress amplitude, and k is a parameter representative of stress biaxiality. The physical meaning of k has been explained on the basis of fracture mechanics [7]. For fatigue limit τ_w in pure torsion, $\sigma_1 = -\sigma_2 = \tau_w$, and the following relation is obtained from Eqn. 2.

$$k = 1 - 1/\phi \text{ or } \phi = 1/(1 - k) \tag{3}$$

where $\phi = \tau_w / \sigma_w$.

For round-bar specimen subjected to combined axial and torsional loading under R = -1, Eqn. 2 is reduced to

$$(1/\phi)^2(\tau_e/\sigma_w)^2 + (1/\phi - 1)(\sigma_e/\sigma_w)^2 + (2 - 1/\phi)(\sigma_e/\sigma_w) = 1 \tag{4}$$

where σ_e is the axial or bending stress amplitude and τ_e is the torsional stress amplitude at fatigue limit under combined loading. Beretta and Murakami [9] predicted ϕ = ~0.83 to 0.87 by stress analysis of a three-dimensional mode I crack emanating from a drilled hole or a hemisherical pit. If ϕ = 0.85 is assumed for round defects such as spherical graphite nodules, a predictive equation is obtained as,

$$1.38(\tau_e/\sigma_w)^2 + 0.176(\sigma_e/\sigma_w)^2 + 0.824(\sigma_e/\sigma_w) = 1 \tag{5}$$

The value of σ_w is predicted by Eqn. 1, so that the fatigue limit stress amplitudes σ_e and τ_e under combined loading are predicted without a fatigue test. Excellent correlations have previously been confirmed between Eqn. 5 and the fatigue data obtained using carbon steel specimens containing an artificial hole and smooth FCD400 specimens containing graphite nodules as inherent small defects [7].

PREDICTION METHOD OF LOWER BOUND FATIGUE LIMIT

Ductile iron has numerous graphite nodules and other small casting defects in the structure. The most detrimental position of a defect in a specimen is in the subsurface very close to the free surface, from the viewpoint of fracture mechanics [10]. Therefore, by assuming the most harmful situation that the largest defect is located just below the surface, the lower bound of the scatter of fatigue limit should be predicted. Murakami and Usuki [10] have proposed the following predictive equation of the lower bound of uniaxial fatigue limit by modifying Eqn. 1.

$$\sigma_{wl} = 1.41\ (HV + 120) / (\sqrt{area}_{max})^{1/6} \tag{6}$$

where σ_{wl} is the lower bound fatigue limit (R = -1) and $\sqrt{area}_{max}$ is the maximum value of $\sqrt{area}$ for the largest defect existing in a given specimen volume. Substituting the Vickers hardness HV of matrix and $\sqrt{area}_{max}$ into Eqn. 6 and then substituting the calculated value of σ_{wl} into σ_w in Eqn. 5, the lower bound fatigue limit under combined loading is expected to be given.

Estimation of the Largest Defect Size

It is virtually impossible to directly measure $\sqrt{area}_{max}$ of the largest defect existing in the specimen interior, even with the most advanced nondestructive inspection method. Here, thus, the statistics of extreme values [11] is employed to predict the value of $\sqrt{area}_{max}$. The prediction method and procedure have been described in detail elsewhere [10,12].

Figure 5 shows microshrinkage cavities observed on the transverse sections of FCD400 and FCD600 specimens. The cavities were present in a ferrite matrix in FCD400, while in FCD600 and FCD700; they were in a pearlite matrix. These cavities are extremely few and the size is usually smaller than or comparable to surrounding graphite nodules when they are observed on a microscope. However, the existence of cavities cannot be ignored from the viewpoint of strength, because a very large cavity is frequently observed on the fatigue fracture origins [2,3]. Figure 7 shows the distributions of the maximum values $\sqrt{area}_{max}$ of graphite nodules and cavities observed in the unit area S_0 =0.500 mm^2. The number of

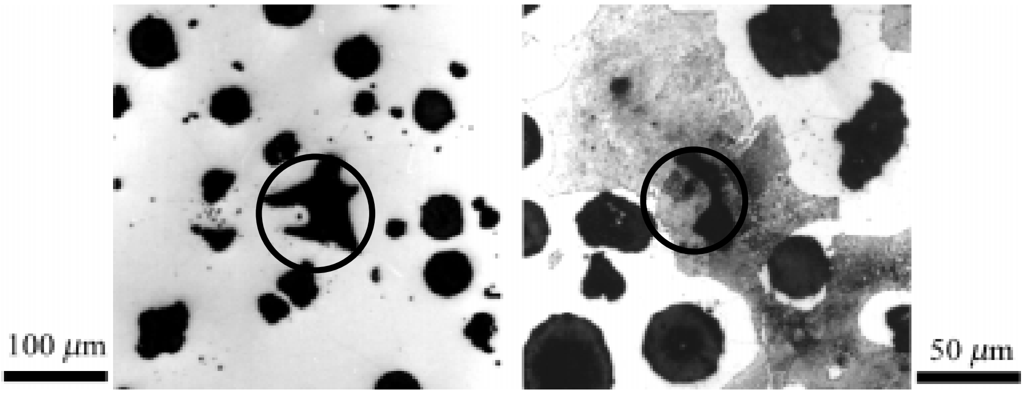

Figure 5: Microshrinkage cavities observed in FCD400 (*left*) and FCD600 (*right*); a rule for estimating $\sqrt{area}_{\max}$ of cavity is also illustrated

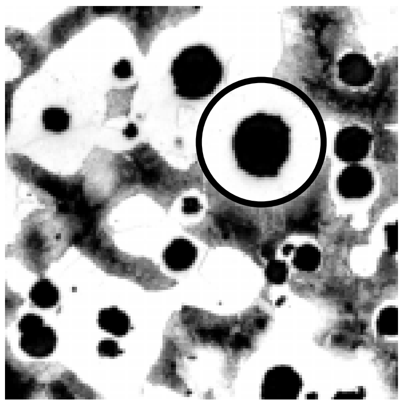

Figure 6: A rule for estimating $\sqrt{area}_{\max}$ of detrimental ferrite matrix

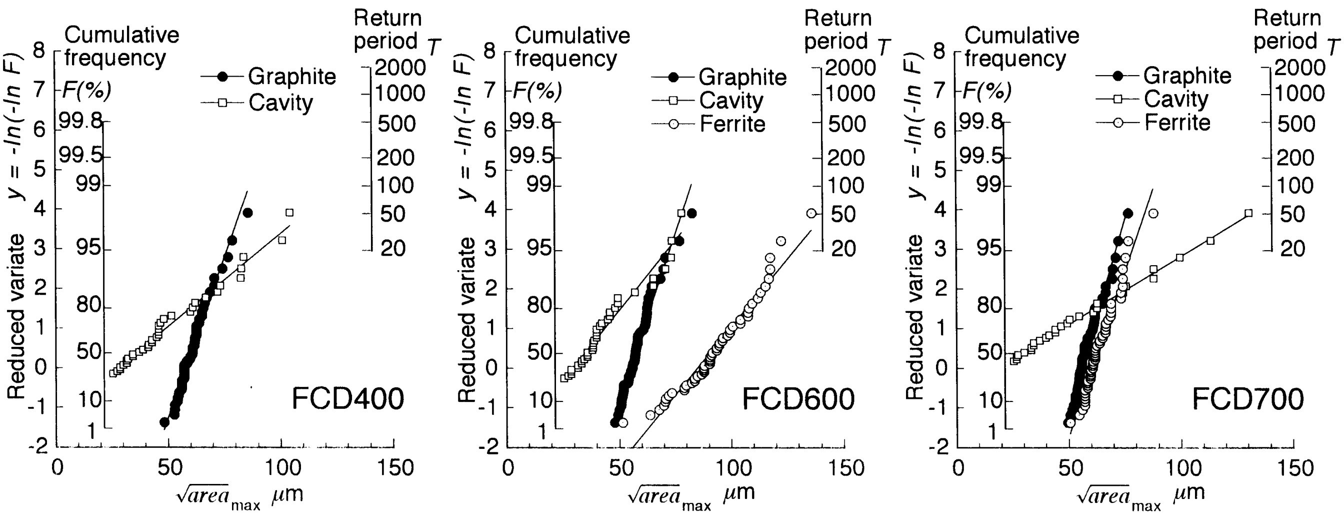

(a) (b) (c)

Figure 7: Cumulative probability distributions of $\sqrt{area}_{\max}$

data is 50 for each. The shape of cavity observed on a plane section is usually irregular, and the area of circumscribed circle of the figure was measured for $\sqrt{area}_{\max}$; see Figure 5. Also it was difficult to identify the cavity when its $\sqrt{area}_{\max}$ was as small as ~25 μm. For such a case, only the number of inspection was counted as frequency assuming the existence of cavity with $\sqrt{area}_{\max} < 25$ μm.

The microstructure of FCD400 is simpler than that of FCD600 or FCD700. Figure 7a indicates that values of $\sqrt{area}_{\max}$ of graphite nodule and cavity obey each different distribution and for a large volume of specimen, cavity can be more harmful than graphite nodule. It is expected that the lower bound fatigue limit of FCD400 be predicted considering competition of graphite nodule and cavity.

In the case of FDC600 and FCD700, an envelope of ferrite surrounds graphite nodule. As typically shown in Figure 3b, a crack initiated from a graphite nodule stops propagating near the grain boundary of ferrite and pearlite. This suggests that the threshold condition of the crack is not only determined by soft ferrite, but also influenced by hard pearlite surrounding the ferrite. In this study, therefore, a ferrite envelope surrounding the largest graphite nodule is regarded as a defect. For this case, $\sqrt{area}_{\max}$ is defined as the square root of the area of inscribed circle in a ferrite matrix containing the largest graphite nodule, as illustrated in Figure 6. Figure 7 shows the distributions of the maximum value $\sqrt{area}_{\max}$ of the inscribed circle in ferrite, which were measured in the unit area S_0 =0.500 mm^2. The number of data is 50. The volume highly stressed in a specimen is 1410 mm^3 for both specimens in Figure 2. Table 2 gives the values of $\sqrt{area}_{\max}$ of the largest defects: nodule, ferrite and cavity, expected for 1, 5 and 10 specimens. The values of $\sqrt{area}_{\max}$ for graphite nodules of FCD600 and FCD700 are not used for prediction but they are listed for comparison with other defect sizes.

Measurement of Hardness

The values of *HV* given in Table 1 were measured with a 10 kg weight, and therefore they are a mean value including the contribution of soft graphite nodules or ferrite. For prediction, the true *HV* values of matrix near the detrimental defect; that is, the *HV* value of ferrite for FCD400 and that of pearlite for FCD600 and FCD700 are necessary. Figure 8 shows the histograms of 100 microhardness values measured with a 25 g weight for FCD400 and with a 50 g weight for both FCD600 and FCD700. The *HV* value shows a large scatter because of soft graphite or ferrite hidden behind the surface. In this study, the value at mostly crowded right end bin of histogram is used as a true hardness. These values are listed in Table 2.

TABLE 2

EXPECTED VALUES OF $\sqrt{area}_{\max}$ AND TRUE VICKERS MICROHARDNESS VALUES

		FC400			FCD600			FCD700		
Number of specimens		1	5	10	1	5	10	1	5	10
$\sqrt{area}_{\max}$, μm	Graphite nodule	125	135	139	119	129	133	112	120	124
	Ferrite	–	–	–	237	260	270	126	136	140
	Microshrinkage cavity	261	295	310	187	210	220	335	382	402
Vickers hardness *HV*		190 (Ferrite)			330 (Pearlite)			330 (Pearlite)		

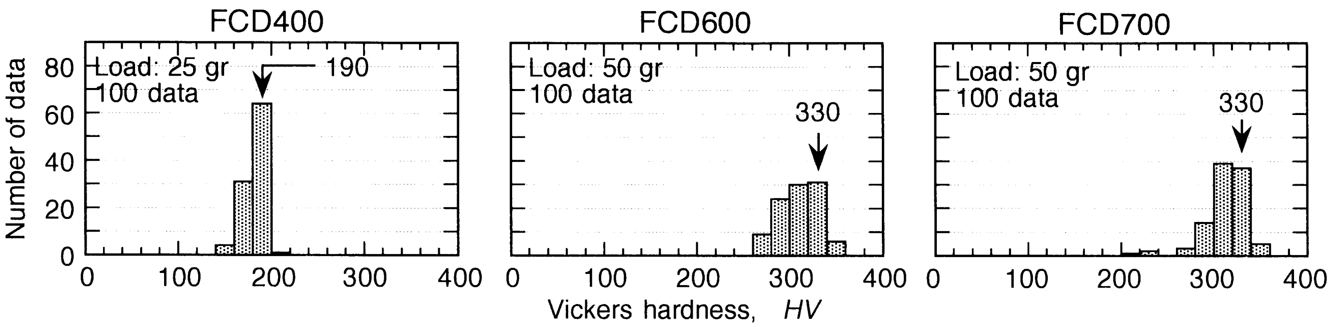

Figure 8: Distributions of Vickers microhardness

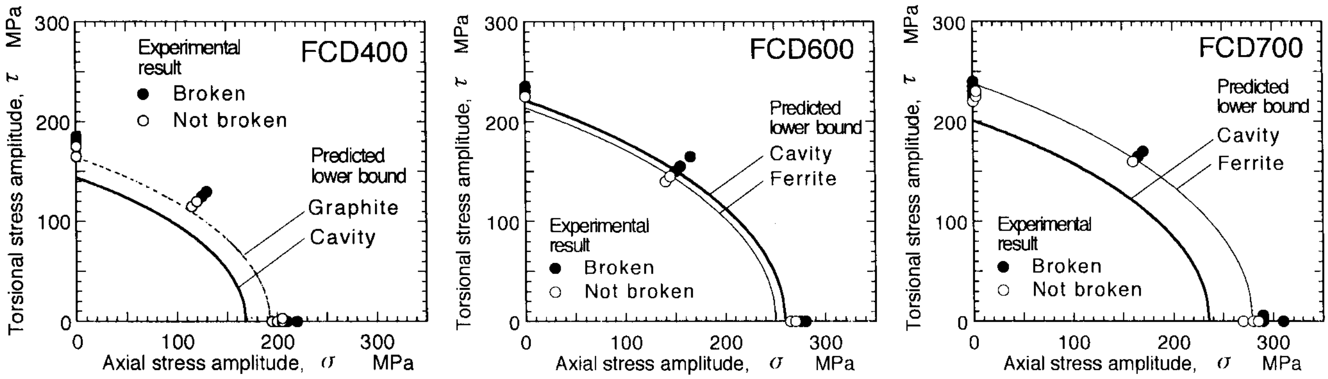

Figure 9: Comparison of predicted lower bound fatigue limits with experimental results

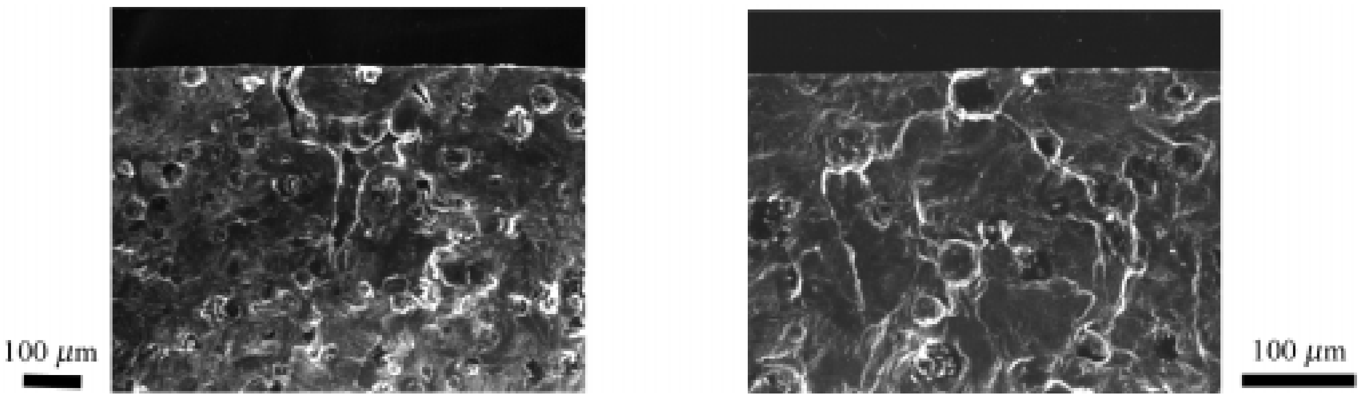

(a) Specimen was broken by τ = 225 MPa at N_f = 2061368 from a microshrinkage cavity

(b) Specimen was not broken by τ = 225 MPa; Fracture surface was obtained retesting at 235 MPa after stress relieving annealing. No large cavity was observed at the fracture origin

Figure 10: Fatigue fracture origins observed in FCD700

DISCUSSION OF THE PREDICTION

Figure 9 shows a comparison of experimental results obtained from 3 to 6 specimens with prediction results of lower bound fatigue limit expected for 5 specimens. Experimental results of FCD400 agree well with the curve predicted using $\sqrt{area}_{\max}$ of graphite nodule and those of FCD600 and FCD700 do well with the curves for ferrite. This is probably because a fairly large defect next to the expected largest defect (nodule or ferrite) is actually present in the specimen subsurface because of an overwhelming majority and it determines the fatigue strength. On the other hand, large microshrinkage cavity is very few, and it may act harmfully to reduce the fatigue strength only when it exists in the subsurface by chance. Hence, care must be exercised when fatigue test is performed with small number of specimens, because it tends to provide a greater value than the true lower bound of fatigue limit.

Figure 10 shows the SEM photographs of fracture surfaces of FCD700 specimens broken in pure torsion tests. The observed planes are inclined 45 degrees to the specimen axis. For both cases, the applied torsional stress is 225 MPa, which is smaller than the lower bound fatigue limit predicted from the largest defect of ferrite (238 MPa) but greater than that predicted from the largest cavity (200 MPa). In the case of Figure 10a, the specimen was broken from a large cavity existing just below the surface. If shape of the cavity is assumed to be a triangle with the surface length of 300 μm and the depth of 340 μm, the value of $\sqrt{area}$ is calculated to be 226 μm and the fatigue limit is predicted to be τ_w = 222 MPa using Eqn. 1 and $\phi = \tau_w / \sigma_w = 0.85$. Thus it is understood that this specimen was to be broken by the applied stress: 225 MPa. In the case of Figure 10b, the specimen did not broken by 10^7 cycles of 225 MPa. This fracture surface was obtained by breaking the specimen at a higher stress (235 MPa) after stress relieving annealing at 600 C in vacuum. No fatal cavity for was observed at the fracture origin, as shown in Figure 10b.

CONCLUSIONS

Ductile iron is cast iron containing graphite nodules and other casting defects such as microshrinkage cavities in the structure. The fatigue strength is influenced by such small defects. In this study, rotating bending and combined axial/torsional fatigue tests were carried out on three kinds of ductile irons: JIS FCD400, FCD600 and FCD700, using round-bar smooth specimens. FCD400 is ferritic iron and FCD700 is pearlitic iron. FCD600 is cast iron with a typical bull's-eye microstructure.

The fatigue limit is determined by the threshold condition for propagation of a mode I crack emanating from small defects. Based on this observation, a criterion for fatigue failure of round-bar specimens with a round defect is proposed as follows:

$$1.38(\tau_e/\sigma_w)^2 + 0.176(\sigma_e/\sigma_w)^2 + 0.824(\sigma_e/\sigma_w) = 1$$

where σ_e is the axial or bending stress amplitude and τ_e is the torsional stress amplitude at fatigue limit under combined loading, and σ_w is the uniaxial fatigue limit. The value of σ_w is predicted in terms of the $\sqrt{area}$ parameter model, so that the fatigue limits σ_e and τ_e are predicted without a fatigue test.

Ductile iron has a number of small defects in the structure. In this study, therefore, the largest graphite nodule and the largest microshrinkage cavity are regarded as detrimental defects for FCD400. For FCD600 and FCD700, the ferrite envelope surrounding the largest graphite nodule and the largest microshrinkage cavity are suspected to be harmful defects. Assuming the most harmful situation that the largest defect is located just below the free surface, the lower bound of uniaxial fatigue limit σ_{wl} is predicted. Then substituting σ_{wl} into σ_w in the above criterion, the lower bound of fatigue limit under combined loading is obtained. The predicted lower bounds are in good agreement with the experimental results

REFERENCES

1. Endo, M. (1997) In: *Proc. Asian Pacific Conf. for Fracture and Strength '96*, pp. 429-433., Korean Soc. Mech. Engrs.
2. Ostensson, B. (1973) *J. Iron and Steel Inst*. Sept., 628.
3. Clement, P., Angeli, J.P. and Pineau, A. (1984) *Fatigue Engng Mater. Struct.* **7**, 254.
4. Murakami, Y. and Endo, M. (1983) *Engng. Fract. Mech.* **17**, 1.
5. Murakami, Y. and Endo, M. (1986) In: *The Behaviour of Short Fatigue Cracks*, pp. 275-293, Miller, K.J. and de los Rios, E.R. (Eds). EMAS Publ., London.
6. Murakami, Y. and Takahashi, K. (1998), *Fatigue Fracture Engng Mater. Struct.* **21**, 1473.
7. Endo, M. (1999) In: *Small Fatigue Cracks: Mechanics, Mechanism and Applications*, pp. 375-387, Ravichandran, K.O., Ritchie, R.O. and Murakami, Y. (Eds). Elsevier, Oxford.
8. Endo, M. (1991) In: *Impact of Improved Materials Quality on Properties, Product Performance, and Design*, *ASME MD-Vol.28*, pp. 125-137, Muralidharan, U. (Ed). ASME, New York.
9. Beretta, S. and Murakami, Y. (1998) In: *Fracture from Defects, Proc. ECF 12,* **I**, pp. 55-60, EMAS Publ., West Midlands.
10. Murakami, Y. and Usuki, H. (1989) *Int. J. Fatigue* **11**, 299.
11. Gumbel, E.J. (1957). *Statistics of Extremes*, Columbia Univ. Press, New York.
12. Beretta, S., Blarasin, A., Endo, M., Giunti, T. and Murakami, Y. (1997) *Int. J. Fatigue* **19**, 319.